

# Ion Diffusion and Acceleration in Plasma Turbulence

F. Pecora<sup>1†</sup>, S. Servidio<sup>1</sup>, A. Greco<sup>1</sup>, W. H. Matthaeus<sup>2</sup>, D. Burgess<sup>3</sup>,  
C. T. Haynes<sup>3</sup>, V. Carbone<sup>1</sup> and P. Veltri<sup>1</sup>

<sup>1</sup>Dipartimento di Fisica, Università della Calabria, I-87036 Cosenza, Italy

<sup>2</sup>Bartol Research Institute and Department of Physics and Astronomy, University of Delaware,  
Newark, DE 19716, USA

<sup>3</sup>School of Physics and Astronomy, Queen Mary, University of London, 327 Mile End Road,  
London, E1 4NS

(Received ?; revised ?; accepted ?. - To be entered by editorial office)

Particle transport, acceleration and energisation are phenomena of major importance for both space and laboratory plasmas. Despite years of study, an accurate theoretical description of these effects is still lacking. Validating models with self-consistent, kinetic simulations represents today a new challenge for the description of weakly-collisional, turbulent plasmas. We perform two-dimensional (2D) hybrid-PIC simulations of steady-state turbulence to study the processes of diffusion and acceleration. The chosen plasma parameters allow to span different systems, going from the solar corona to the solar wind, from the Earth's magnetosheath to confinement devices. To describe the ion diffusion, we adapted the Nonlinear Guiding Center (NLGC) theory to the 2D case. Finally, we investigated the local influence of coherent structures on particle energisation and acceleration: current sheets play an important role if the ions Larmor radii are on the order of the current sheets size. This resonance-like process leads to the violation of the magnetic moment conservation, eventually enhancing the velocity-space diffusion.

**PACS codes:** Authors should not enter PACS codes directly on the manuscript, as these must be chosen during the online submission process and will then be added during the typesetting process (see <http://www.aip.org/pacs/> for the full list of PACS codes)

---

## 1. Introduction

Processes such as turbulence, diffusion and particle acceleration are ubiquitous both in astrophysical and laboratory plasmas. Understanding particle diffusion is of fundamental importance in order to characterize the distribution of the charged gas in the universe and, more specifically, in the heliosphere. The understanding of the energetic particle motion, originating, for example, from solar flares or coronal mass ejections, can help to prevent injuries for space travelers, as well as hardware damages for satellites. Moreover the distribution of heavy ions in the Earth's magnetosphere can have effects on climate changes (Luo *et al.* 2017). Particle transport theory is fundamental for the dynamics of the solar corona (Lepreti *et al.* 2012) and of the interplanetary medium (Ruffolo *et al.* 2003, 2004). In laboratory plasma experiments, the magnetic confinement could be improved by understanding what affects particle turbulent transport (Taylor & McNamara 1971; Hauff *et al.* 2009).

<sup>†</sup> Email address for correspondence: francesco.pecora11@unical.it

Charged particle dynamics depends on the stochastic motion of the magnetic field lines. The random walk of the magnetic field lines affects the diffusion both across and along the mean magnetic field (Jokipii & Parker 1969). Charged particles gyrate along the magnetic field but, if the field is turbulent, they spread in the perpendicular direction (Ruffolo *et al.* 2012; Chandran *et al.* 2010), “jumping” from a field line to another. The turbulent nature of space and laboratory plasmas suggests that the best way to describe their dynamics is given by the statistical approach (Green 1951; Jokipii 1966). In this statistical (Lagrangian) description, particles move in a turbulent electromagnetic field, similarly to the motion of neutral tracers in atmospheric turbulence (Richardson 1926; Kolmogorov 1941). The turbulent nature of the fields that scatter the particles limits the analytical treatment of the subject. For this, we still lack an exact and universal theory for describing the perpendicular diffusion (Bieber & Matthaeus 1997; Hussein & Shalchi 2016).

A common theoretical approach, applied when studying diffusion of charged particles, relies on calculating separately the diffusion coefficient in directions parallel and perpendicular to the main guiding field (Jokipii 1966; Subedi *et al.* 2017). Currently the NLGC theory (Matthaeus *et al.* 2003) gives a rather accurate prediction of the diffusion coefficient for systems with a three-dimensional (3D) geometry. However, this theory has been tested only with test-particle simulations - simulations that do not take into account the back-reaction of the particles motion on the electromagnetic fields. Nowadays, more realistic simulations of turbulence are available and is therefore interesting to test the validity of these predictions, using, for example, kinetic models.

A full 3D description of plasma turbulence requires huge computational efforts that can be lightened by reducing the dimensionality of the problem. Magnetohydrodynamics (MHD) turbulence simulations (Dobrowolny *et al.* 1980; Shebalin *et al.* 1983; Dmitruk *et al.* 2004) have shown that, if a strong guiding magnetic field is present, turbulence loses the property of isotropy. The magnetic structures are mainly present in the plane perpendicular to the main field (Bruno & Carbone 2016). These structures are essentially composed by a sea of flux tubes (magnetic islands) and current sheets, where reconnection might eventually occur (Matthaeus & Lamkin 1986; Greco *et al.* 2009*a*; Servidio *et al.* 2011*b*). In this complex pattern, particles diffuse and accelerate.

MHD simulations suggest that turbulence can be considered as a network of reconnecting magnetic islands, that merge, change topology and convert energy (Parker 1957; Matthaeus *et al.* 1984; Ambrosiano *et al.* 1988; Servidio *et al.* 2009). Magnetic reconnection is considered one of the most effective mechanisms for particle acceleration and energisation (Zank *et al.* 2014*a*), being crucial for explosive events in the solar atmosphere, like solar flares (Cargill *et al.* 2006, 2012; Cadavid *et al.* 2014) and coronal mass ejections (Gosling 2010). Analogously, in the Earth’s magnetosphere (Drake *et al.* 2006; Oka *et al.* 2010; Birn *et al.* 2012) and far away to the heliopause (Lazarian & Opher 2009), magnetic reconnection is thought to be a very active mechanism. Observations and measurements strongly relate the magnetic island merging (Zank *et al.* 2014*b*) and the magnetic field discontinuities (Tessein *et al.* 2013) with the increase of suprathermal energetic particles. This increasing number of energetic particles in zones of merging magnetic islands and of strong discontinuities can be the key interpretation to relate the magnetic reconnection with acceleration and energisation (le Roux *et al.* 2015; Lazarian & Opher 2009).

Both 2D and 3D simulations of MHD turbulence with a strong guiding magnetic field (Matthaeus & Lamkin 1986; Gray & Matthaeus 1992; Dmitruk *et al.* 2004) reveal power law energy spectra for test-particles. The power-law spectra can be indeed observed for anomalous cosmic rays (Stone *et al.* 2008; Decker *et al.* 2010), energetic ions in the solar wind (Fisk & Gloeckler 2006) and energetic electrons in solar flares (Holman *et al.*

2003). It is worth noting, however, that since test-particle models are not self-consistent, particles in these simulations can reach extremely high energies. These very high energies might not be commonly observed in the solar wind, in usual turbulence conditions, especially for ions, suggesting that a self-consistent kinetic model need to be used in order to correctly describe the plasma dynamics.

The present work is organized as follows. In Section 2 we will present a global overview on the model that describes the plasmas in the low-collisionality limit. We will introduce the numerical algorithm that simulate the plasma-particle dynamics. In Section 3, the particle trajectory statistics will be presented, interpreting the numerical results via the plasma turbulent diffusion theories. The investigation of the acceleration process will be the central topic of Section 4, where we will perform local analysis of the acceleration phenomenon. Finally, in the last Section, we will present the discussions, conclusions and future perspectives.

## 2. Simulations of 2D Plasma Turbulence

We perform three hybrid-PIC simulations, varying the plasma  $\beta$  (the ratio between kinetic and magnetic pressure), with  $\beta = 5, 0.5$  and  $0.1$ , in order to cover a wide range of relevant plasma scenarios. These chosen values are such that the high  $\beta$  value is typical of plasmas found in the Earth's magnetosheath; the value of  $\beta = 0.5$  is close to the typical solar wind conditions, whereas the lowest  $\beta$  is appropriate for the the solar corona and laboratory devices.

Particles and fields are described by the Vlasov-Maxwell system Eq.s 2.1 that we solve via a hybrid-PIC approach, using kinetic ions and fluid electrons. The system of equations is given by

$$\begin{aligned}
 \dot{\mathbf{x}} &= \mathbf{v} \\
 \dot{\mathbf{v}} &= \mathbf{E} + \mathbf{v} \times \mathbf{B} \\
 \frac{\partial \mathbf{B}}{\partial t} &= -\nabla \times \mathbf{E} \\
 \mathbf{E} &= -(\mathbf{u} \times \mathbf{B}) + \frac{1}{n} \mathbf{j} \times \mathbf{B} - \frac{1}{n} \nabla P_e + \eta \mathbf{j}.
 \end{aligned} \tag{2.1}$$

In the above equations,  $\mathbf{x}$  is the particles position,  $\mathbf{v}$  their velocity,  $\mathbf{E}$  is the electric field,  $\mathbf{B}$  is the magnetic field,  $\mathbf{u}$  is the proton bulk velocity (the first moment of the velocity distribution function),  $n$  is the proton number density (the zero-th moment of the ion velocity distribution function),  $\mathbf{j}$  is the current density. The pressure term is adiabatic  $P_e = \beta n^\gamma$  and  $\eta = 0.006$  is the resistivity that introduces a small scale dissipation, for numerical stability. The electric field is given by the generalised Ohm's law. In the simulations distances are normalized to  $c/\omega_{p_i}$ , where  $c$  is the speed of light and  $\omega_{p_i}$  is ion plasma frequency. The time is normalized to  $\Omega_{c_i}^{-1}$ , that is the ion cyclotron frequency. Finally, velocities are normalized to the Alfvén speed  $v_A = c\Omega_{c_i}/\omega_{p_i}$ .

The three simulations have the same initial conditions: uniform density and a Maxwellian distribution of particles velocities with uniform temperature. We impose large scale fluctuations in order to mimic the motion of the large energy-containing vortices. We have chosen random fluctuations, at large scale, for both magnetic field and the ion bulk velocity field. The Eq.s 2.1 are solved on a square grid of size  $L_0 = 128d_p$ , where  $d_p$  is the proton skin depth defined as  $d_p = c/\Omega_{c_i}$ , discretized with  $512^2$  points, with periodic boundary conditions. This initial state consists of a 2D spectrum of fluctuations, perpendicular to the main field  $B_0$  (the latter chosen along  $z$ ). The fluctuations amplitude is

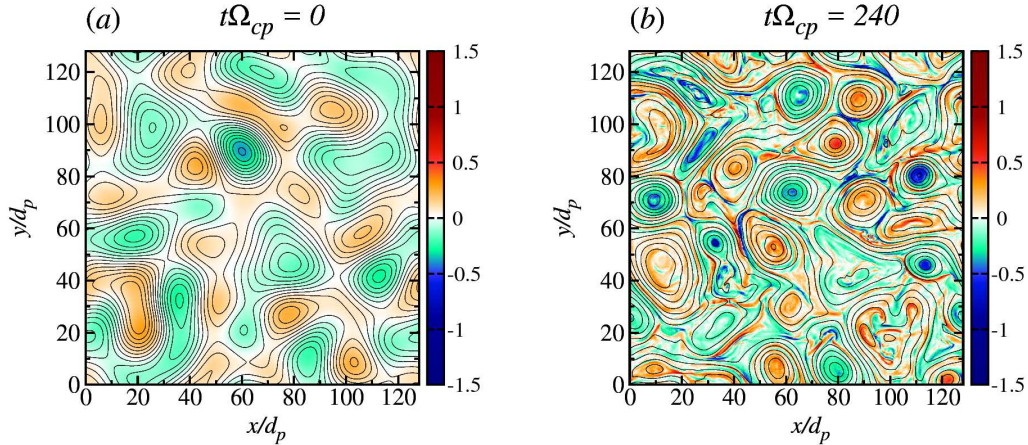


Figure 1: Current density  $j_z$  (colour map) together with vector potential  $a_z$  (contour lines), at the initial state (a), with big structures and tenuous axial current, and at the final state (b), with coherent structures such as small vortices and intense current sheets. The most intense current sheets are located in between reconnecting magnetic islands (Matthaeus 1980).

$\delta b/B_0 \sim 0.3$ . To suppress the statistical noise of the PIC method we use 1500 particles per cell (about  $4 \times 10^8$  total particles).

To describe the magnetic topology, in the 2.5D approximation, it is useful to define the in-plane magnetic field as  $\mathbf{B}_\perp = \nabla a_z \times \hat{\mathbf{z}}$ , where  $a_z$  is the magnetic potential and  $\hat{\mathbf{z}}$  is the out-of-plane (axial) unit vector. The current in the axial direction  $j_z = (\nabla \times \mathbf{B}_\perp) \cdot \hat{\mathbf{z}} = -\nabla^2 a_z$ . To achieve a stationary state of fully developed turbulence, we initially let the system decay freely, and then we introduce a forcing at the time  $t^*$  at which nonlinearity reaches its peak (roughly the peak of  $\langle j_z^2 \rangle$ ), namely  $t^* \sim 25\Omega_{cp}^{-1}$ . The forcing consists of “freezing” the amplitude of the large-scale modes of the in-plane magnetic field, with  $1 \leq m \leq 4$ , with constant phases. This corresponds to a large-scale input of energy, as described in Servidio *et al.* (2016).

In order to have a significant statistics, we perform our analysis when a steady state has been achieved, namely for  $50 < t\Omega_{cp} < 250$ . Fig. 1 shows the shaded contour of the current density  $j_z$  along with the contour line of the vector potential  $a_z$ , as the system evolves toward turbulence. Panel (a) shows the initial state of the system, where islands and current sheets are not defined yet. As time goes on, smaller vortices and sharp current sheets develop. In particular, these magnetic structures represent magnetic islands (flux tubes in 3D). The global appearance of the system remains unchanged, in a statistical sense, when the peak of nonlinearity has been reached. The regions of big magnetic gradient appear in between reconnecting magnetic islands, with associated intense current sheets (Matthaeus 1980; Servidio *et al.* 2015).

To better describe the state of fully developed turbulence, we computed the Fourier spectra, as a function of the wavenumber  $|\mathbf{k}|$ , of both the electric and magnetic fields. The power spectra for the trace of the correlation tensor,  $|\hat{\mathbf{B}}(\mathbf{k}, t)|^2$ , where  $\hat{\mathbf{B}}(\mathbf{k}, t)$  are the respective Fourier coefficients, are reported in Fig. 2. These spectra exhibit the classical scenario of MHD turbulence, in which energy flows from large to small scales. This cascade of energy occurs over the so-called inertial subrange, where energy that scales as  $k^{-5/3}$  (Bruno & Carbone 2016). In particular, Fig. 2 shows the turbulent development. The state of fully developed turbulence is achieved after  $50\Omega_{cp}^{-1}$ . After this time the spectra

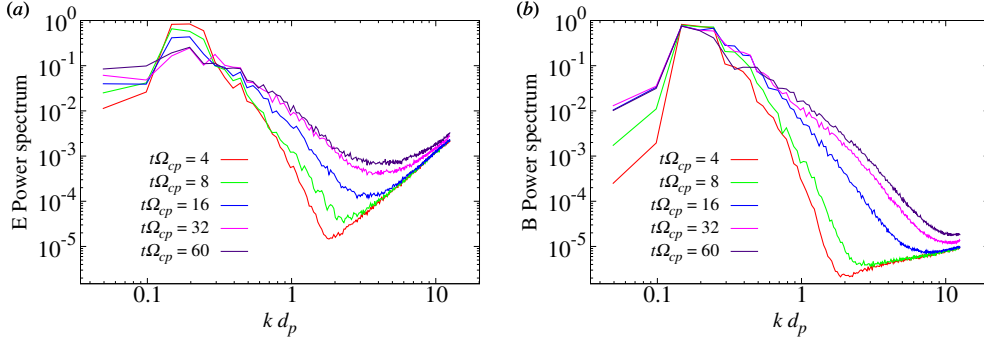


Figure 2: Power spectra of electric (a) and magnetic (b) fields as a function of the wavenumber (normalized with the proton skin depth  $d_p$ ), at different times. While turbulence develops, energy is transferred from the large to the small scales. In the steady state, at  $k \sim d_p^{-1}$ , the electric field spectrum manifests a steeper slope.

are almost stationary (do not experience large fluctuations). It is important to note, that as observed in the solar wind (Bale *et al.* 2005), the power in the electric fields is higher, at  $k$ 's that correspond to characteristic ion lengths. This is in agreement with previous studies and simulations of plasma turbulence (Howes *et al.* 2008; Matthaeus *et al.* 2008; Franci *et al.* 2015).

In order to understand the dynamics of particles in a turbulent scenario, where structures are present at different scales, it is useful to measure different characteristic lengths. The correlation (or integral) length of a turbulent field generally corresponds approximately to the size of the largest energy-containing turbulent eddies, (in our case the typical sizes of the islands.) This length can be obtained from the two-point correlation function  $C(\mathbf{r})$  as

$$\lambda_C = \int_{\Omega} C(\mathbf{r}) d\mathbf{r} = \frac{1}{\langle b^2 \rangle} \int_{\Omega} d\mathbf{r} \langle \mathbf{b}(\mathbf{x} + \mathbf{r}) \cdot \mathbf{b}(\mathbf{x}) \rangle. \quad (2.2)$$

Here  $\mathbf{b}$  represents the magnetic fluctuations and  $\langle \cdot \rangle$  is the average over the total volume  $\Omega$ . Note that fluctuations are isotropic in the plane perpendicular to the main field, hence  $\mathbf{x}$  and  $\mathbf{r}$  are in-plane vectors and the above length is essentially the same, namely  $C(r_x) \sim C(r_y) \equiv C(\mathbf{r})$ . Moreover,  $\lambda_C$  is very similar for the bulk velocity fluctuations, because of the choice of the initial conditions and the driving. In the above definitions we suppressed the time dependence because of stationary, and we computed these lengths averaging over time, in the steady state regime. For our system  $\lambda_C \sim 10d_p$  and does not vary for runs with different plasma  $\beta$ .

Apart of the above energy-containing scale, which is a large scale characteristic length of turbulence, it is important to characterize also the smallest scales properties. In hydrodynamics the Taylor length is the scale at which the viscous dissipation term is no longer negligible (Servidio *et al.* 2011b). This scale is related to the largest width of the structures, where dissipation starts to be relevant. In our case, the magnetic Taylor scale can be defined as

$$\lambda_T = \sqrt{\frac{b_{\perp}^2}{\langle j_z^2 \rangle}}. \quad (2.3)$$

In the above expression,  $b_{\perp}$  is the root mean square of the magnetic field in the plane perpendicular to the axial direction (perpendicular to the main guiding field), and  $\langle j_z^2 \rangle$

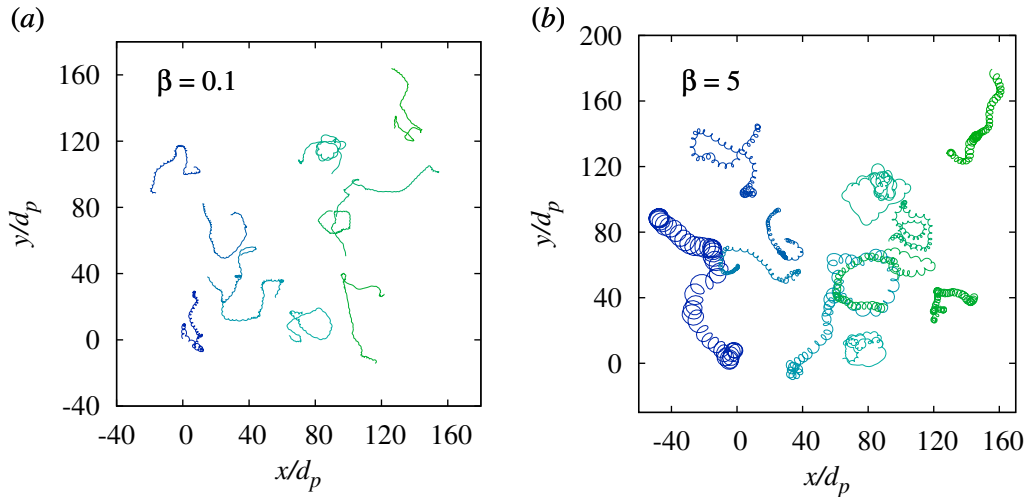


Figure 3: Particle trajectories for different values of  $\beta$ , namely  $\beta = 0.1$  (a) and  $\beta = 5$  (b). It is possible to observe that particles in high  $\beta$  have bigger Larmor radii, while particles in low  $\beta$  move almost on straight lines, with more abrupt change of direction. One can notice some particles have closed orbits like they are trapped in a magnetic island while others experience turnovers that suddenly bend the trajectory.

is the axial current averaged over the 2D space, and averaged also over the times in which the system is in the stationary state of fully developed turbulence. This scale can be considered as the scale at which the inertial range of turbulence terminates (Frisch 1995). In our simulations  $\lambda_T \sim 1.7d_p$ . Since the Taylor length  $\lambda_T$  gives the biggest size of the dissipative structures, we introduce now an average measure of these structures, namely the typical width of the layer cores (O-points). The current sheet width,  $\delta_c$ , is the half maximum width of the current sheet intensity profile. The average core width of the current sheets we measured as  $\delta_c \sim 0.3d_p$ .

### 3. Particle diffusion in plasma turbulence

We investigate the particle motion in steady state turbulence. Among all PIC macroparticles, we have followed the path of  $10^5$  samples, verifying the convergence of the statistical results. From their positions as a function of time, it is possible to compute the diffusion coefficient, measuring their mean squared displacement. After a general overview on the erratic trajectory of particles in 2D turbulence, we will see whether the plasma  $\beta$  affects the statistics of ions diffusion and acceleration.

In Fig. 3 we show the 2D trajectories of some randomly selected particles, during the whole simulation, for two distinct values of  $\beta$  (low and high  $\beta$ ). As it can be seen, particles that move in high  $\beta$  plasma are less magnetized and their Larmor radii is large. Particles in low- $\beta$  plasma, instead, are highly magnetized and perform tight gyrations, with more abrupt change of direction. Small- $\beta$  particles spread less than in the high  $\beta$  case. Generally, in all cases, one can notice that some particles have closed orbits as they are trapped in a magnetic island while others experience turnovers that suddenly bend the trajectory. As we shall see, particles that perform closed trajectories are mostly trapped in turbulent vortices, whereas sharply segmented trajectories can belong to particles which

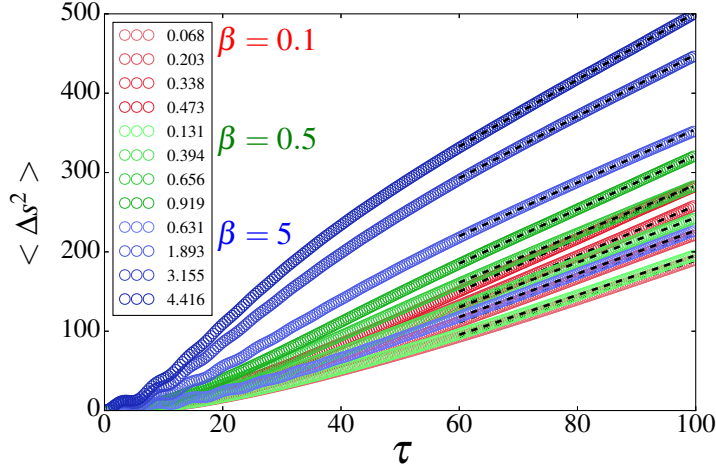


Figure 4: Mean squared displacement in the perpendicular plane as a function of the time  $\tau$  (cyclotron units), for several particles energy ranges. For small times, it is possible to observe a deviation from the linear prediction of the Brownian motion (Eq. 3.1). Normal diffusion is achieved at later times, for  $\tau > 60\Omega_{cp}^{-1}$ , where we extrapolate the values of  $D$  via linear fits (dashed lines).

encounter local intense turbulent structures, as magnetic discontinuities or current sheets, that make them deviate suddenly (Drake *et al.* 2010; Haynes *et al.* 2014).

The overall motion, as represented in Fig. 3, seems quite random: particles scatter and diffuse in time. We computed the square displacement  $\Delta s^2 = \Delta x^2 + \Delta y^2$ , finding that, for sufficiently long time intervals, the motion is diffusive, namely

$$\langle \Delta s^2 \rangle = 2D\tau. \quad (3.1)$$

In the above expression,  $D$  is the diffusion coefficient,  $\tau$  is the time interval over which the particle moves by  $\Delta s$ , and the brackets now represent an ensemble average computed over particles. Note that  $\tau = t - t_0$ , and because of stationarity we varied  $t_0$  in the range of the steady state regime. To understand the dependence of the diffusion coefficient on particle energy, we divide the particles in energy bins and evaluate the above diffusion coefficient, collecting particles depending their average energy. The averaged mean squared displacement as a function of the time interval for several energy values is shown in Fig. 4. It is possible to observe the normal diffusive behavior is achieved for for  $\tau \gtrsim 60\Omega_{cp}^{-1}$ . By fitting the curves after this interval with the Eq. 3.1, we can obtain the numerical value of  $D$ . For shorter time intervals particles seems to not follow the linear law. Indeed, for short time intervals the particle motion cannot be stochastic since they have “memory” of their initial condition, and temporal correlations exist. It is clear that the higher is the particles energy, the larger is the diffusion coefficient. Before reporting the numerical results on the diffusion of particles in self-consistent kinetic simulations, we will introduce the theoretical background.

### 3.1. A Non Linear Guiding Center (NLGC) model in 2D

We want to develop a theory that can describe particle diffusion in 2D turbulence, and test it with the self-consistent plasma simulations. Currently, a useful description of perpendicular diffusion is given by the Non Linear Guiding Center (NLGC) theory (Matthaeus *et al.* 2003). This theory works well for 3D turbulence, with a uniform mean

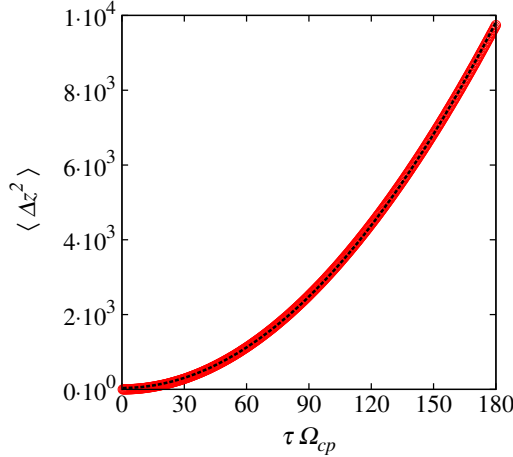


Figure 5: Mean squared displacement in the  $z$  direction averaged over all particles as a function of  $\tau$ . The dashed line is the parabolic fit ( $\propto \tau^2$ ). For every  $\beta$ , the assumption of free streaming made in Eq. 3.2 is pretty solid.

magnetic field, and it has been tested with test-particle simulations. To develop the 2D version of the theory we start from the 3D NLGC derivation, considering the particle gyromotion. Using the Taylor-Green-Kubo (TGK) formulation (Taylor 1922; Green 1951; Kubo 1957; Shalchi & Dosch 2008; Shalchi 2015), one can write the diffusion coefficient  $D_{xx}$ , for instance along the  $x$  direction, as

$$D_{xx} = \frac{1}{B_0^2} \int_0^\infty d\tau \langle v_z(0) B_x(\mathbf{x}(0), 0) v_z(\tau) B_x(\mathbf{x}(\tau), \tau) \rangle,$$

where it is assumed that the particle motion projected on the 2D plane follows the 2D projection of the magnetic field lines. We assume that the magnetic field fluctuations in the perpendicular plane are completely uncorrelated with the velocity in the  $z$  direction and this allows us to write the diffusion coefficient as

$$D_{xx} = \frac{1}{B_0^2} \int_0^\infty d\tau \langle v_z(0) v_z(\tau) \rangle \langle B_x(\mathbf{x}(0), 0) B_x(\mathbf{x}(\tau), \tau) \rangle.$$

Now we encounter a deviation from the 3D NLGC, by saying that the velocity correlation function in the  $z$  direction is nothing but the square value of the  $z$  velocity i.e.

$$\langle v_z(0) v_z(\tau) \rangle \sim v_z^2. \quad (3.2)$$

This assumption has been directly proved by measuring the quantity  $\langle v_z(0) v_z(\tau) \rangle$  in our simulations. Fig. 5 shows that the motion along  $z$  is given by free streaming, with  $\langle \Delta z^2 \rangle \sim t^2$  and therefore the velocity  $v_z$ , in the direction along the main field, is almost constant.

Using this approximation, we can estimate the diffusion coefficient neglecting the parallel scattering, and get:

$$D_{xx} = \frac{v_z^2}{B_0^2} \int_0^\infty d\tau \langle B_x(\mathbf{x}(0), 0) B_x(\mathbf{x}(\tau), \tau) \rangle.$$

Using the Corrsin's independence hypothesis to transform the integrand function as

$$\langle B_x(\mathbf{x}(0), 0) B_x(\mathbf{x}(\tau), \tau) \rangle = \int d\mathbf{r} R_{xx}(\mathbf{r}, \tau) P(\mathbf{r}, \tau)$$



one arrives at

$$D_{xx} = \frac{v_z^2}{B_0^2} \int_0^\infty d\tau \int d\mathbf{r} R_{xx}(\mathbf{r}, \tau) P(\mathbf{r}, \tau),$$

where  $R_{xx}(\mathbf{r}, \tau)$  is the Eulerian two-point two-time correlation tensor and  $P(\mathbf{r}, \tau)$  is the probability function of the particle having displacement  $\mathbf{r}$  after a time interval  $\tau$  (Matthaeus *et al.* 2003). At this point is convenient to express  $R_{xx}(\mathbf{r}, \tau)$  using its Fourier transform

$$R_{xx}(\mathbf{r}, \tau) = \int d\mathbf{k} S_{xx}(\mathbf{k}, \tau) e^{i\mathbf{k}\cdot\mathbf{r}}.$$

We can model  $S_{xx}(\mathbf{k}, \tau) = S_{xx}(\mathbf{k})\Gamma(\mathbf{k}, \tau)$ , where  $\Gamma(\mathbf{k}, \tau)$  represents the time-propagator of the spectrum, and  $S_{xx}(\mathbf{k})$  is spatial spectrum. Usually, this functional form is described via the so-called sweeping decorrelation mechanism, namely  $\Gamma(\mathbf{k}, \tau) \sim e^{-\tau/\tau_c(\mathbf{k})}$ , where  $\tau_c(\mathbf{k})$  is a characteristic decorrelation time. The latter is usually thought to be the “sweeping decorrelation time” (Chen & Kraichnan 1989; Nelkin & Tabor 1990), in analogy with fluid turbulence (see below).

At this point, we can proceed with the theoretical estimate of the diffusion coefficient, given by

$$D_{xx} = \frac{v_z^2}{B_0^2} \int_0^\infty d\tau \int d\mathbf{k} S_{xx}(\mathbf{k}) d\tau \Gamma(\mathbf{k}, \tau) \int d\mathbf{r} P(\mathbf{r}, \tau) e^{i\mathbf{k}\cdot\mathbf{r}}. \quad (3.3)$$

Since  $P$  is Gaussian, then

$$\int d\mathbf{r} P(\mathbf{r}, \tau) e^{i\mathbf{k}\cdot\mathbf{r}} = e^{-(k_x^2 D_{xx} + k_y^2 D_{yy})\tau}.$$

In In axisymmetric turbulence  $D_{xx} = D_{yy} \equiv D$ ,  $S_{xx} = S_{yy} \equiv S$  and, since we have only in-plane structures (i.e.  $k_z = 0$ )  $k_x^2 + k_y^2 \equiv k^2$ , the diffusion coefficient is

$$D = \frac{v_z^2}{B_0^2} \int d\mathbf{k} S(\mathbf{k}) \int_0^\infty d\tau e^{-k^2 D \tau} e^{-\tau/\tau_c(\mathbf{k})}.$$

Finally, integrating over  $\tau$ , one gets

$$D = \frac{v_z^2}{B_0^2} \int d\mathbf{k} \frac{S(\mathbf{k})}{[\tau_c(k)]^{-1} + k^2 D}. \quad (3.4)$$

Note that this prediction is only a small modification to the NLGC theory, having suppressed the  $z$ -dependence by using the particle free streaming along  $z$  (Eq. 3.2).

In order to obtain a first estimate of the diffusion coefficient  $D$ , we can make an approximation. Assuming that the sweeping decorrelation time is rather long, (as in the case of large scale slow driving, for example) we can drop the term  $\tau_c(k)^{-1}$  in Eq. 3.4. This latter term, indeed, makes the equation more complex to solve. We therefore obtained:

$$D^* \sim \sqrt{\frac{v_z^2}{B_0^2} \int d\mathbf{k} \frac{S(\mathbf{k})}{k^2}}. \quad (3.5)$$

The reader may notice that this result is essentially of the same form as the so-called Field Line Random Walk (FLRW) limit of perpendicular particle scattering (Jokipii 1966; Bieber & Matthaeus 1997). For such cases,  $D = v_{eff} D_{fl}$  where  $D_{fl}$  is the Fokker Planck coefficient for field line transport, and  $v_{eff}$  is the effective velocity of the particle along the magnetic field (Matthaeus *et al.* 1995).

To evaluate the diffusion coefficient via Eq. 3.5 and Eq. 3.4, we computed the average power spectrum  $S(\mathbf{k})$ , from the simulations. Fig. 6 shows the numerical values of  $D$

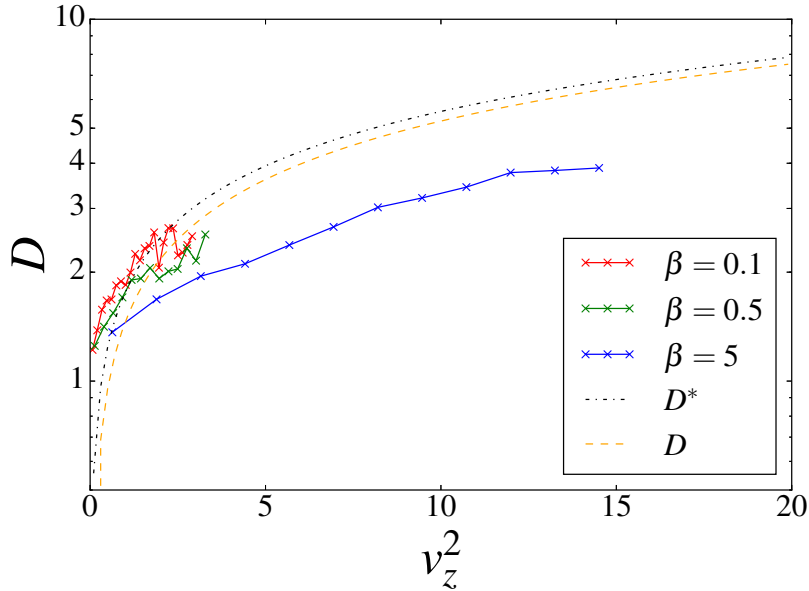


Figure 6: The diffusion coefficient as a function of the parallel energy  $v_z^2$ , calculated by fitting the mean square displacement (red, green and blue line-points respectively for  $\beta = 0.1, 0.5$  and 5) for all the simulations. The theoretical diffusion coefficient from the approximated 2D NLGC theory (Eq. 3.5) is reported with the black point dashed line whereas the exact calculation (Eq. 3.4) is the orange dashed line.

obtained by fitting the particles mean squared displacements in Fig. 4. The theoretical values of the 2D NLGC, evaluated via both the exact and the approximated formulas, are reported as a function of the particles energies. The simulations results follow fairly well the theoretical prediction at low  $\beta$ . The theory slightly deviates at very high energy ( $\beta$ 's), although the functional monotonic behaviour is very similar. We will note that we do not observe large energy excursions like in test-particle models, due to the self-consistency of the ions treatment.

Here we briefly investigate the decorrelation mechanism in self-consistent, plasma turbulence. We performed a Fourier transform in time of the magnetic fluctuations, computing the propagator  $\Gamma(k, \tau)$ , as described in Ref.s (Servidio *et al.* 2011a; Perri *et al.* 2017). As in fluid, MHD, and Hall MHD models of turbulence, this time-dependent correlation of turbulence strongly depends on the amplitude of  $k$ , as reported in Fig. 7. As it can be seen, the decorrelation mechanism depends on  $k$  and drops quickly in time (only a few inertial range modes are reported). From this functional form, we computed the decorrelation time  $\tau_C(k)$ , represented in the panel (b) of the same figure. The decorrelation time scales as  $\sim 1/k$ , indicating the clear dominance of the sweeping effect. To be more quantitative, in order to compute the diffusion coefficient for our experiment, we found that  $\tau_C(k) \sim 3/(\delta b_\perp k d_p)$ , where  $\delta b_\perp$  is the *rms* of the in-plane magnetic fluctuations.

#### 4. Particle Acceleration

In agreement with previous literature (Jokipii & Parker 1969; Matthaeus *et al.* 2003), we have found that diffusivity depends on particles energy. The behavior of diffusion is in agreement with a modified model of the NLGC theory, here adapted to collisionless

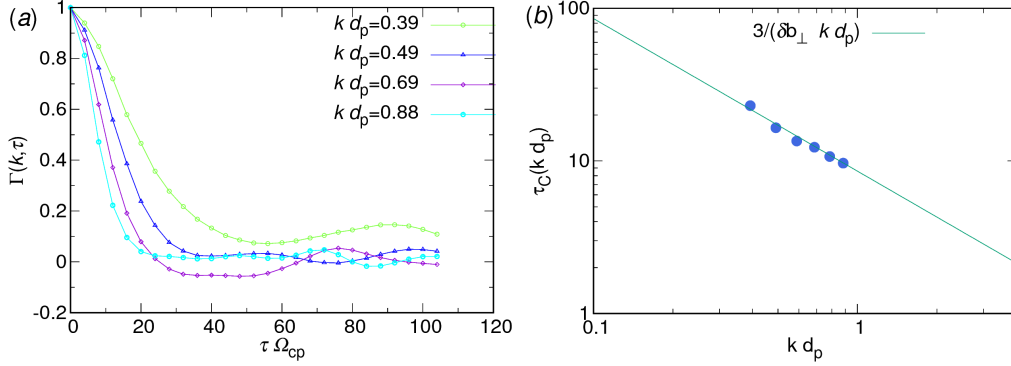


Figure 7: (a) Propagator of the magnetic field spectrum, computed for several (perpendicular)  $k$  modes in the inertial range of plasma turbulence. (b) Decorrelation time as a function of  $k$  (blue bullets), computed as the  $e$ -folding time of the functional form in panel (a). The sweeping prediction is reported with dashed (green) lines.

2D plasmas. Moreover, we observed that many of these particles experience variations of their momentum – namely an acceleration process. In this section, we investigate the mechanisms responsible for acceleration, using conditional statistics. We will establish the relationship between the effectiveness of the acceleration mechanism and the particle energies, and the existence of possible resonance conditions that energize the ions.

We have computed, for each particle, the Lagrangian acceleration  $\mathbf{a} = \partial \mathbf{v} / \partial t$ , where  $\mathbf{v}$  is the particle velocity. We computed the the Probability Distribution Function (PDF) of the Lagrangian acceleration, for all the particles, at different times and for different simulations. The acceleration has been computed by using a 6<sup>th</sup> order finite difference (centered) method. The distributions are reported in Fig. 8, for the two extreme  $\beta$ , at the beginning and at the end of the simulation. As it can be observed, the PDFs of particle acceleration in high  $\beta$  plasma are well described by the  $\chi^2$  distribution. Let  $\{x_1, x_2, \dots, x_k\}$  be a set of  $k$  independent normally distributed variables. The sum of the square of these  $k$  variables distributes according to the  $\chi_k^2$  PDF that is defined as

$$PDF(\chi_k^2) = \frac{1}{2^k \Gamma(k/2)} x^{k/2-1} e^{-x/2}$$

where  $k$  are commonly referred to as degrees of freedom, and  $\Gamma(x)$  is the gamma function. In our case the three independent variables are the acceleration components  $\{a_x, a_y, a_z\}$  and the square modulus of the acceleration  $|a|^2 = a_x^2 + a_y^2 + a_z^2$  distributes according to the  $\chi_3^2$  with 3 degrees of freedom.

For  $\beta = 5$ , in particular, this distribution does not change in time, indicating the lack of very extreme events during the evolution of the system. Whereas at low  $\beta$  ( $\beta = 0.1$ ), the acceleration, which is initially randomly distributed, develops a tail at later times (blue solid line). This means that the number of particles with anomalous acceleration is higher for low  $\beta$  plasma, suggesting that a physical process that depends on the plasma conditions is at work.

A straightforward acceleration mechanism can be due to an electric field parallel to the local magnetic field:

$$E_{\parallel} = \frac{\mathbf{E} \cdot \mathbf{B}}{|\mathbf{B}|}. \quad (4.1)$$

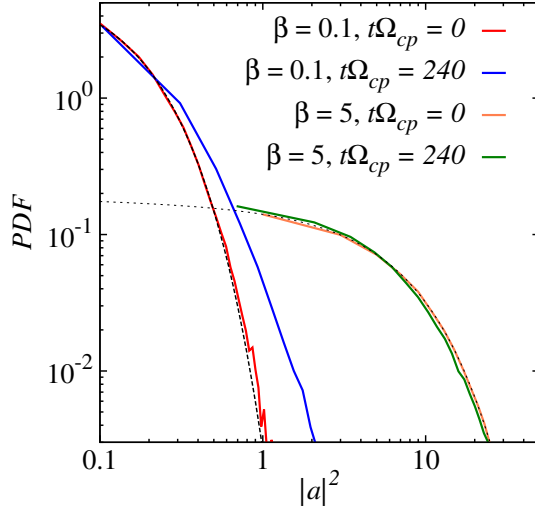


Figure 8: PDFs of the acceleration, for  $\beta = 0.1$  and  $\beta = 5$ . Both initial and final times of the simulations are reported, together with the corresponding probability distributions (dashed black lines). In the low beta case, extreme acceleration processes are observed.

We identified the anomalous particles, i.e. the particles with acceleration values exceeding the variance of the followed distribution and represented their positions, at a given time, over the parallel electric field map with a contour plot of the magnetic potential in the  $z$  direction, in order to see whether they show a correlation with the turbulent structures. This map is reported in Fig. 9. The figure shows that particles with anomalous acceleration are affected by the above field: accelerating ions are non uniformly distributed, they cluster where the parallel electric field is more intense, on the flanks of the magnetic islands.

In order to establish a more quantitative link between the parallel electric field and possible local acceleration effects, we compared the PDFs of the single terms of the electric field that can be parallel to the local magnetic field (namely  $\nabla P_e$  and  $\eta j$ ) and of the total parallel electric field itself ( $E_{\parallel}$ )

over the positions of non-anomalous particles, and the PDFs of the same quantities measured only at the positions of high-acceleration particles. The particles were distinguished by thresholds with respect to the global acceleration PDF: the anomalous particles are those which have an acceleration value exceeding the  $3\sigma$  of the global distribution, whereas “normal” particles have an acceleration value within  $1\sigma$ . Note that the above conditional statistics would give the same distribution only if acceleration and  $E_{\parallel}$  are uncorrelated. These PDFs are shown in Fig. 10, where the quantities with superscript  $\uparrow$  are measured at the positions of anomalously accelerated ions, whereas the fields with superscript  $\downarrow$  are related to “normal” particles. As it can be seen, accelerated particles have higher parallel electric field – the population of the distribution is higher at big  $E_{\parallel}$  regions. Moreover we used the Partial Variance of Increments (PVI) method to find candidate regions likely to be identified as coherent structures. These structures contribute to non-Gaussian statistics and therefore to intermittency. The PVI time series is substantially defined as the normalized sequence of magnetic increments. By applying the PVI technique, we found that the regions of bigger  $E_{\parallel}$  occur in correspondence of magnetic discontinuities and not in smooth regions, as the PDF of  $E_{\parallel}$  conditioned on PVI values (Greco *et al.* 2009b) clearly evidences in the inset of panel (a) of Fig. 10.

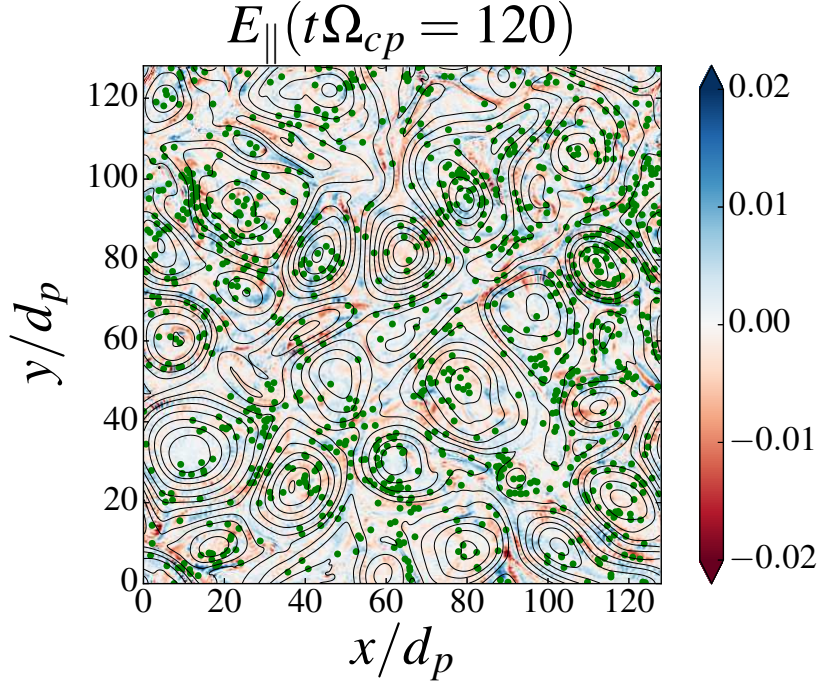


Figure 9: Particles with very high acceleration (green dots), superimposed on the shaded contour of the parallel electric field. These particles are localized in the regions where the parallel electric field is bigger.

This statistics further confirm the relation between the parallel electric field and the stochastic acceleration mechanisms in 2D turbulence.

This acceleration mechanism in the out-of-plane direction has a global effect of elongating the ion velocity distribution function (VDF). In order to see if this typical alignment effect is present in our numerical experiments, we computed both the PDF of the angle between particles velocity and the local magnetic field and the PDF of the angle the particles velocity has with the main magnetic field (along  $z$ )

$$\cos(\theta) = \frac{\mathbf{v} \cdot \mathbf{B}}{|\mathbf{v}||\mathbf{B}|}, \quad \cos(\psi) = \frac{v_z}{|\mathbf{v}|} \quad (4.2)$$

In Fig. 11 we report the distributions of both the angles, at the initial and final times of the simulation, for different values of  $\beta$ . At the initial time, when turbulence is very “young”, the distributions are quite flat, meaning particles are moving isotropically. As the simulation goes on, particles tend to align with the main magnetic field in the  $z$  direction. This effects is much more evident for the low  $\beta$  plasma, the more magnetized one. Another feature one can notice in the low  $\beta$  plasma is that the particles orient themselves more on the local magnetic field rather than its  $z$  component, although the  $z$  component is its main one and the difference is not statistically relevant.

It is crucial to see now whether this acceleration mechanism, locally related to intense parallel electric fields, can actually increase the particles energy, and up to which values. This correspondence is not trivial since the particles with anomalous acceleration are only a small fraction of the plasma. We have constructed the energy PDF to see whether the energy has a different behavior at different  $\beta$ . The energy PDFs for the low and high

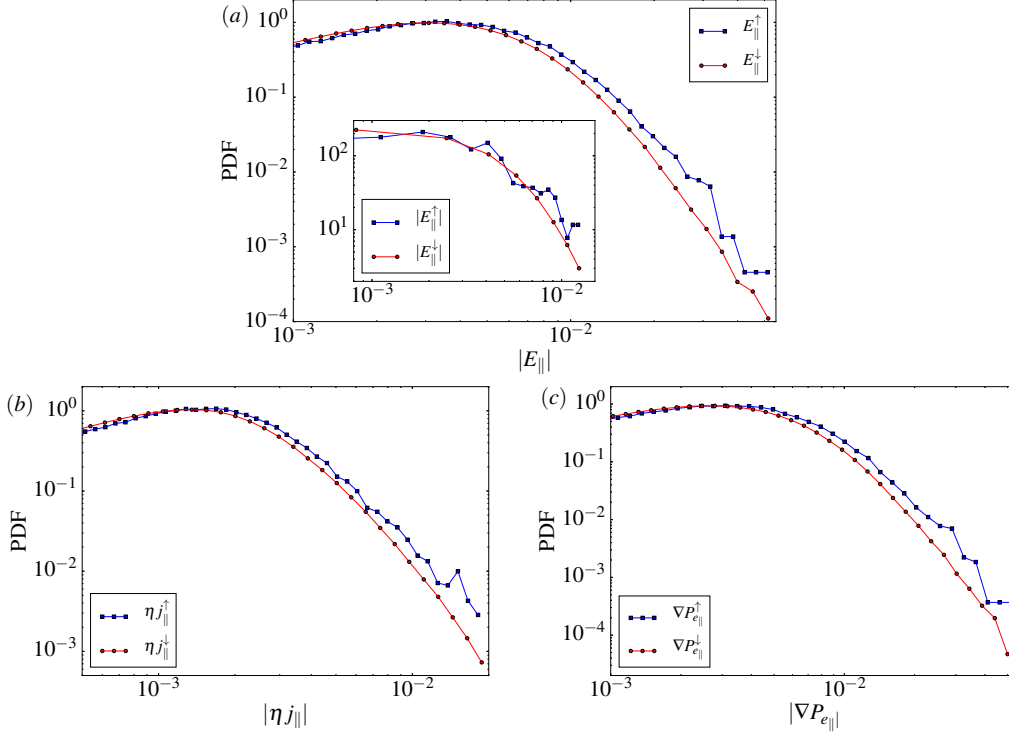


Figure 10: Conditioned PDFs of the electric field  $E_{\parallel}$  (a) and of its single components  $\eta j$  (b) and  $\nabla P_e$  (c) in the direction parallel to the local magnetic field. The condition is related to the particles acceleration values. In particular, the fields with superscript  $\uparrow$  (blue dots) are measured at the position of particles with acceleration exceeding  $3\sigma$ , whereas the fields labeled with  $\downarrow$  (red dots) are measured where particles with acceleration less than  $1\sigma$  lie. The whole parallel electric field and both its component show the same behaviour: anomalous particles are more likely to be found where the field values are bigger. This indicates that particles cluster close to regions where dynamical activity is occurring near current sheets, suggesting an association with magnetic reconnection. The inset of panel (a) shows the total parallel electric field component conditioned over the PVI values. The red circles are the parallel electric field values computed along the whole PVI path, whereas the blue squares are the parallel electric field values computed in the regions where the PVI exceeds a threshold value. This correlation indicates that high electric field values are more probable to be found where magnetic field inhomogeneities are stronger.

$\beta$  values are show in Fig. 12. In the low  $\beta$  scenario, the PDF develops a power law tail, already seen in observation and previous numerical simulations. Whereas in the high  $\beta$  plasma the energy remains similar to the initial distribution, namely close to Maxwellian distribution. This suggests that the acceleration mechanism can energize particles, and that the process depends on the plasma  $\beta$ .

#### 4.1. Magnetic Trapping

We have seen that the acceleration mechanism involves the parallel electric field. However, there must be something else that makes this field energizing particles in low  $\beta$  plasmas.

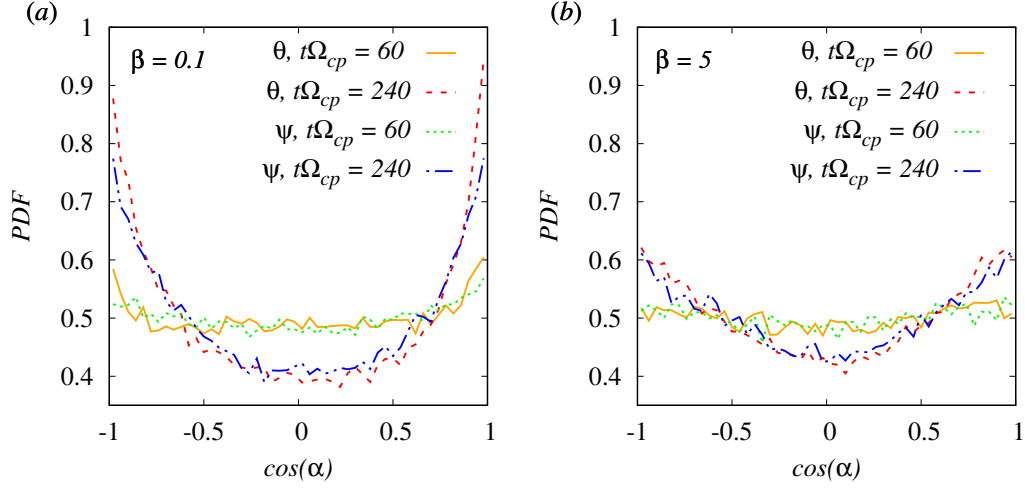


Figure 11: PDFs of the cosine of the angle between the particles velocity and the magnetic field for low (a) and high (b)  $\beta$  values at the initial and final instants of the simulation. The orange (solid) and red (dashed) lines represent the PDF of the angle the velocity forms with the local magnetic field at the initial and final time respectively. The green (dotted) and blue (solid-dotted) ones represent the angle that particles velocity forms with the main magnetic field in the  $z$  direction at the same two instants. Both the two plasma scenarios start with an isotropic distribution of the velocities with respect to the magnetic field. Then the less magnetized particles (low  $\beta$  plasma) become strongly aligned with the magnetic field. The same effect is evident, though much less pronounced, for less magnetized particles (low  $\beta$  plasma).

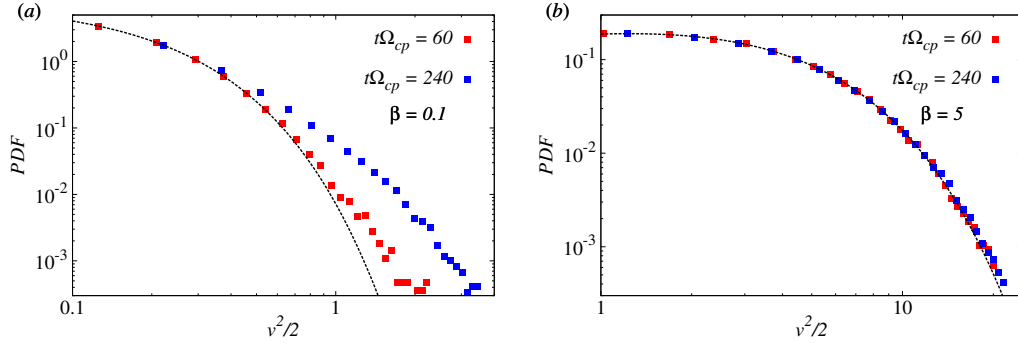


Figure 12: PDF of the particles energy, for the high and low  $\beta$  simulations, at different times of the simulation. The high  $\beta$  distribution does not change during the simulation, whereas the low  $\beta$  particles have a substantial energy gain because of turbulence.

In figure Fig. 9 we have seen that the anomalous particles lie within (or in between) magnetic islands, in agreement with previous discussions. The acceleration mechanism, evidently occurs in association with magnetic reconnection. Particles temporarily trapped inside small flux tubes or in the dynamically active region of larger flux tubes experience Fermi-like processes. In the region near current sheets, particles can experience nearly continuous first order energisation (Hoshino *et al.* 2001; Drake *et al.* 2010; Haynes *et al.*

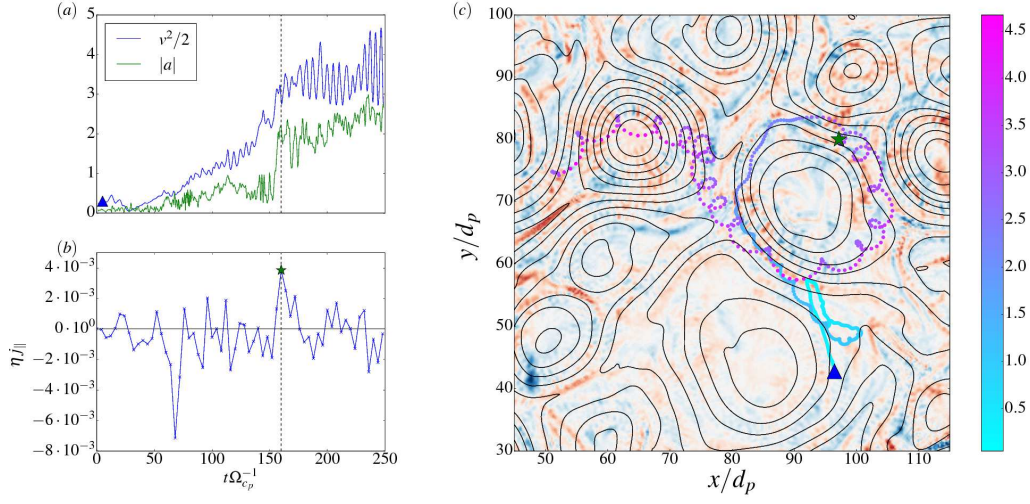


Figure 13: One of the most energetic particles followed along its path. Panel (a) shows the particle energy and its acceleration. All of them show an increase in correspondence of a peak in the parallel current density reported in (b). Panel (c) shows the colour map of the parallel electric field with the particle path which colour represents the particle's energy. The colour clearly shows that the particle gets energized when it remains trapped in the magnetic island until it gets enough energy to escape. The blue triangle represents the starting point of the trajectory and the green star is the point where the maximum value of parallel current density is found.

2014). In particular we followed the trajectory of one of the most energetic particles and monitored its energy, its acceleration, the energy derivative with respect to time and the parallel current density it samples during its journey (the parallel pressure term is not shown because it is too noisy for non-statistical treatment) (Fig. 13). The figure also shows that the particle remains trapped in a magnetic island and its energy grows until it reaches a high enough energy to escape.

To estimate the escaping times we calculated the Lagrangian auto-correlation time using Eq. 4.3. This quantity represents the time at which each particle experience a correlated field, and can be estimated as

$$T_{esc} = \frac{1}{\langle v_x(t_0)^2 \rangle_a} \int_0^\infty \langle v_x(t_0)v_x(t_0 + \tau) \rangle_a d\tau. \quad (4.3)$$

In the above definition, the operation  $\langle \cdot \rangle_a$  is the average only over the particles that have high acceleration. For the usual isotropy hypothesis, we computed the above relation along all directions, finding similar results. We obtained the following escaping times:  $T_{esc}^{anom}(\beta = 5) \sim 0.8\Omega_{cp}^{-1}$ ,  $T_{esc}^{anom}(\beta = 0.5) \sim 3.0\Omega_{cp}^{-1}$ , and  $T_{esc}^{anom}(\beta = 0.1) \sim 5.7\Omega_{cp}^{-1}$ . In addition we computed the same quantity for *all* the particles, obtaining these values:  $T_{esc}^{all}(\beta = 5) = 0.95\Omega_{cp}^{-1}$ ,  $T_{esc}^{all}(\beta = 0.5) = 4.13\Omega_{cp}^{-1}$ ,  $T_{esc}^{all}(\beta = 0.1) = 9.64\Omega_{cp}^{-1}$ . This scenario is consistent with the fact that particles in low  $\beta$  plasmas develop high energy tails, since they are confined within magnetic islands for longer periods, experiencing the same parallel electric field. On the other hand, particles in high  $\beta$  plasmas easily escape from magnetic islands and are not efficiently energized. The comparison of the trapping times values at the same  $\beta$  for the different kind of particle populations also supports this view. The escaping times calculated over all the particles are bigger than those of the



anomalous particles suggesting that more energetic particles are more likely to escape from magnetic islands while lower energy particles remain trapped for longer period and can be coherently energised. This Fermi-like process, invoked in small scale reconnection (Ambrosiano *et al.* 1988), is now quantitatively observed in large scale plasma turbulence. It is interesting now to further characterize the energisation process by looking at the characteristic parameters of these anomalous particles.

#### 4.2. The Magnetic Moment

We now further inspect the acceleration process by looking at the magnetic moment  $\mu$  of ions, defined as

$$\mu = \frac{mv_{\perp}^2}{2B}. \quad (4.4)$$

In the above expression,  $m$  is the particle mass and  $v_{\perp}$  its velocity (perpendicular to the magnetic field  $\mathbf{B}$ , measured at the particle's position).  $\mu$  is an adiabatic invariant of the system, if  $B$  is slowly varying. Indeed, the orbits are like closed circles and the flux of magnetic field passing through them is almost constant. This suggests that the magnetic moment might not be a constant of the motion in a turbulent system where several spatial scales are present, and where magnetic field variations are neither negligible nor adiabatic (Dalena *et al.* 2012). To quantify the behaviour of the magnetic moment for each particle, we computed the normalized moment

$$\tilde{\mu}_p = \frac{\mu_p(t) - \mu_p(0)}{\mu_p(0)}, \quad (4.5)$$

where the label  $p$  now indicates a single particle. This measure gives us information about the variation of the particle magnetic moment with respect to its initial value. Fig. 14 shows  $\tilde{\mu}_p$  as a function of time, for some particles, randomly selected, for two plasma  $\beta$  values. Particles that moves in low  $\beta$  plasma have the highest magnetic moment excursions, while in the high  $\beta$  plasma, where particles are not so energized in time, their magnetic moment is much more conserved. It is important to notice that the magnetic moment distribution is very similar to the distribution of energies and acceleration, further confirming the relevance of this quantity for the process of plasma acceleration in turbulence.

To see whether the magnetic moment is a constant of the motion, in a more quantitative way (Fig. 14 refers only to a small portion of particles), we calculated the standard deviation  $\sigma_{\mu}(p)$ . This can be interpreted as the dispersion of the magnetic moment, for each particle, and is defined as

$$\sigma_p = \sqrt{\frac{1}{T} \int_{t_0}^{t_0+T} [\mu_p(t') - \langle \mu_p \rangle_T]^2 dt'}, \quad (4.6)$$

where  $\mu_p(t)$  is the magnetic moment of the  $p$ -th particle at the time  $t$ , and the average in the integral is calculated over the whole time. In case of a perfectly conserved magnetic moment, this quantity is null. We have then built the PDF of

$$\varepsilon = \frac{\sigma_p}{\langle \mu_p \rangle_t}, \quad (4.7)$$

that indicates how much the magnetic moment deviates from its mean value – how much the magnetic moment is “broken”. The PDF( $\varepsilon$ ) is shown in panel (a) of Fig. 15. As expected, the violation of the magnetic moment is much more pronounced (broader distribution) in the case of  $\beta = 0.1$ . Low- $\beta$  particles have small gyro-radii and they can probably interact with the local strong inhomogeneities.

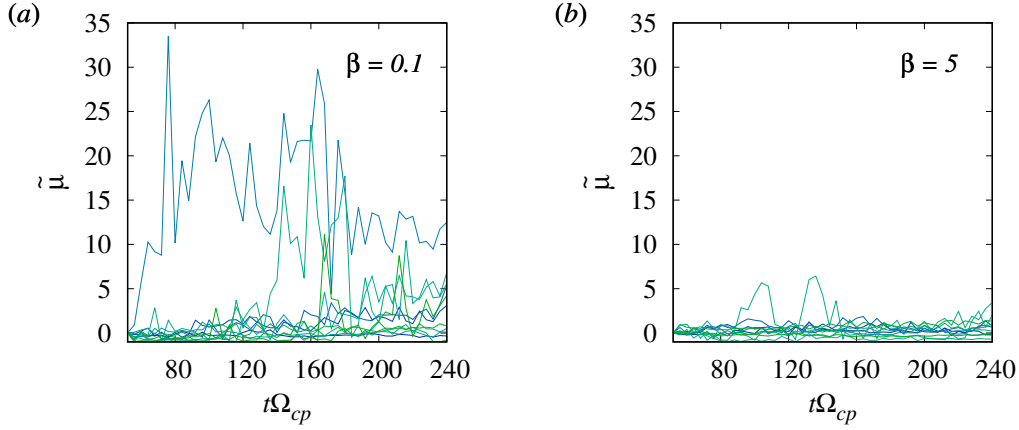


Figure 14: Magnetic moment as a function of time, for a group of 11 particles (same as in Fig. 16), for two values of  $\beta$ . In high- $\beta$  plasma (b), the magnetic moment is much more constant (conserved).

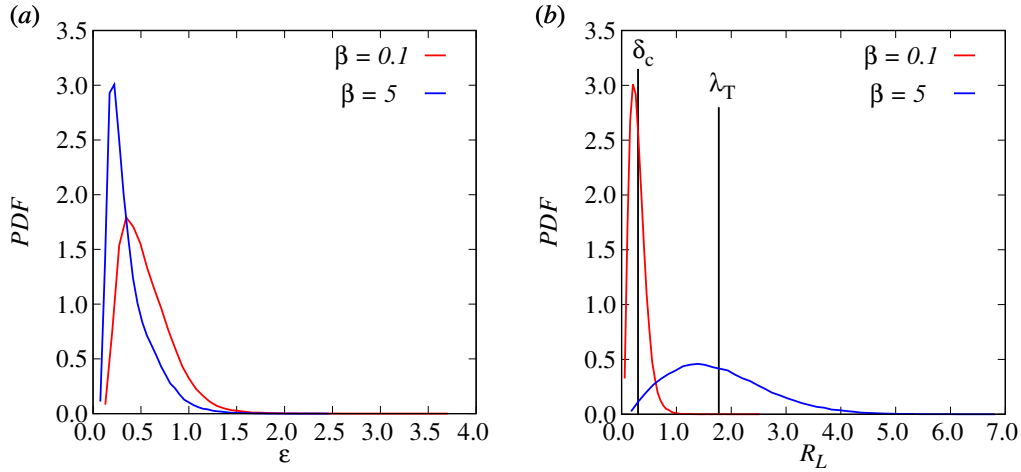


Figure 15: (a) PDF of the dispersion of the magnetic moment defined in Eq. 4.7. These PDFs show that particles are more likely to “break” their magnetic moment in the low  $\beta$  case. (b) PDF of the Larmor radius for different  $\beta$ 's. High  $\beta$  particles have a wide distribution, reaching values up to one order of magnitude bigger than in the low- $\beta$  case. The Taylor length  $\lambda_T$  and the current width  $\delta_c$  are also indicated. The Taylor length indicates the length of the biggest current sheet in the plane and sets an upper limit to the particles that can effectively get energized by interacting with the current sheets. Whereas the current width  $\delta_c$  is the average current sheet thickness.

We can relate the magnetic moment violation directly to the turbulence characteristic scales. Our analysis suggests that particles can interact with current sheets, if their Larmor radius is much shorter than the Taylor length  $\lambda_T$  – the largest current sheet size (Eq. 2.3). If the radius is bigger, the particle can gyrate without even “noticing” the current sheet. The other important scale is the current width  $\delta_c$ , that is the mean size of the current sheet cores. Panel (b) of Fig. 15 shows a more quantitative view of the above speculation, suggesting a kind of spatial resonance. In this figure we report the

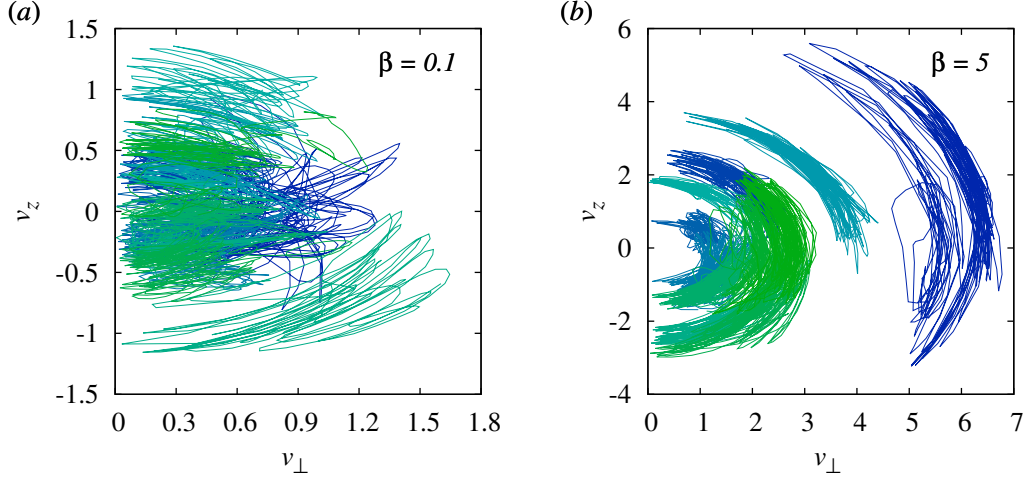


Figure 16: Velocity space trajectories for the particles of Fig. 14, at high and low  $\beta$ 's. Particles moving in the high  $\beta$  plasma are more energetic and do not undergo energisation processes. They diffuse in pitch angle and hence move on quasi-isoeenergetic shells. Differently, in the low  $\beta$  scenario, particles manifest more complex (ergodic) trajectories: they are not locked on isoeenergetic shells as they can effectively gain/lose energy throughout their magnetic islands journey.

PDF of the Larmor radius along with the turbulence characteristic lengths  $\lambda_T$  and  $\delta_c$ . The Larmor radii of particles in high  $\beta$  plasma are broadly distributed and are much bigger than the current sheets thickness (while they are on the order of the Taylor scale). The case with  $\beta = 0.1$  shows, instead, that the average  $R_L$  are smaller than (or on the order of)  $\delta_c$ . In this scenario, particles with the resonant Larmor radius feel the presence of the sharp discontinuities, and undergoes a magnetic moment break. This finally leads to the acceleration mechanism, and to the energisation of ions in turbulent plasmas.

#### 4.3. Approaching to Velocity Space Diffusion

We have studied the process of particles acceleration and energisation. Acceleration can be interpreted as a “motion” in the velocity space, i.e.  $v$ -diffusion (Subedi *et al.* 2017). In this last section we will briefly mention this aspect of diffusion. As for spatial diffusion, it is instructive to observe particles trajectories in the velocity space. In particular, we represent these trajectories in a 2D space made by  $v_z$  (parallel to the global magnetic field) and the in-plane velocity  $v_\perp = \sqrt{v_x^2 + v_y^2}$ . The trajectories in the velocity space are shown in Fig. 16.

The velocity space trajectories show, from another point of view, the same behavior we have seen in the previous sections. In the high  $\beta$  plasma, particles are accelerated but not effectively energized by the parallel electric field. This means that they can diffuse only in pitch-angle and gyrophase, namely they move on the surface of iso-energetic shells, varying only the angle the velocity forms with the magnetic field. In the low  $\beta$  scenario, particles, instead, are accelerated and energized by the current sheets. The combined acceleration and energisation phenomena make particles trajectories in the velocity space more complex, since particles can diffuse both in pitch-angle and momentum-amplitude. In this case, ions change their velocity modulus and can acquire a continuous range of values making the trajectories almost ergodic. The ergodicity domain is bounded by

the upper limit of energy a particle can gain before escaping a vortex and run into a decelerating (de-energizing) electric field. This interesting aspect of diffusion will be further inspected in future works.

## Discussion and Conclusions

In this work we described the diffusion and the acceleration of ions in plasma turbulence, using self-consistent kinetic simulations (kinetic ions and fluid electrons). These topics are of primary importance both in astrophysical and laboratory plasmas. We simplified the problem by using a 2D geometry, which can be a valid approximation to understand the nature of strongly anisotropic (magnetized) fluctuations (Shebalin *et al.* 1983; Dmitruk *et al.* 2004; Matthaeus & Lamkin 1986). Particles have been evolved making use of a PIC algorithm. The PIC algorithm is very useful and of practical fundamental importance when treating non-equilibrium plasmas for which the wave-particle interactions are crucial. The 2D hybrid-PIC simulations have been performed for three different  $\beta$ 's, in order to reproduce a wide range of physical systems. The different values of  $\beta$  used vary for more than one order of magnitude allowing us to describe plasma scenarios spanning from the solar corona to fusion devices. The 2D maps of the current density along with the magnetic field showed the development of fundamental turbulent structures, such as vortices and current sheets.

We have then studied the motion of ions, moving self-consistently in the electromagnetic field. As suggested by previous (and numerous) test-particles studies, the motion is very erratic. Particles can be trapped in magnetic vortices or scattered away by current sheets, wandering like a pollen in the atmosphere (Servidio *et al.* 2016), or field lines in the solar corona (Rappazzo *et al.* 2017). This kind of trajectories are achieved after rather long time intervals and can be statistically described within the theory of diffusion. The particle motion becomes uncorrelated when the particle is no longer trapped by the same vortex. Low energy particles have been found to have longer correlation times as they cannot easily escape from vortices.

All the existing theories on the diffusion coefficient can describe 3D systems and all these theories have been verified only with test-particle models. The NLGC theory is possibly the most precise theory that gives an estimate of the diffusion coefficient. We have then “reduced” this theory to the 2D case. This 2D NLGC theory has been found to be valuable in describing the diffusion coefficient of particles moving in self-consistent turbulent fields.

From the acceleration process, the PDFs show that the acceleration nature depends on the plasma  $\beta$ . Acceleration is a stochastic variable for high  $\beta$  plasmas, whereas it is distributed with power-law tails for low  $\beta$  case. We have found that the electric field component parallel to the magnetic field is correlated with particle acceleration. The “anomalously” accelerated particles, i.e. the particles with acceleration values that exceed the variance of the distribution, are connected to regions with high parallel electric field. This has been seen, qualitatively, by spotting these particle on the parallel electric field map and, quantitatively, by computing the conditional statistics.

By looking at the energy PDFs, we noticed that particles in low  $\beta$  systems, such as in the solar wind, are more effectively energized. This process can be linked to the presence of narrow current layers. The main phenomenon acting on the particle is the breaking of the particle magnetic moment. Local spatial resonances break this constant of motion, leading to acceleration and finally to energisation of particles. In this process, particle undergo a spatial resonance with the background turbulent structures: ions that have their Larmor radius on the order of the current sheet thickness experience large excursions

of their magnetic moment. These particles experience a local acceleration process, while in the case with much larger  $\beta$ , as can be found in the magnetospheric environment, the plasma elements do not “see” the reconnecting current sheets and the embedded parallel electric field. This kind of interaction with vortices and current sheets has been proved also by looking at characteristic scales resonances. Particles characteristic scale is the Larmor radius, whereas for turbulence we computed the Taylor length and the current width. A consistent percentage of high energy particles has a Larmor radius bigger than the Taylor length, that is, qualitatively, the in-plane length of the biggest current sheet. This means high energy particles can barely “notice” the current sheets.

Finally, we have introduced the concept of velocity space diffusion, because above processes might be related to the stochastic motion of particles in the velocity space. We still lack a fundamental theory to determine the diffusion coefficient in velocity space (Miller *et al.* 1990; Miller & Roberts 1995), and we leave this work for future studies. Future works can be focused on an analytical treatment of the velocity-space diffusion. Moreover, a full 3D study will be performed in the future, taking into account also the role of kinetic electrons.

## Acknowledgments

This work is partly supported by the International Space Science Institute (ISSI) in the framework of International Team 405 entitled “Current Sheets, Turbulence, Structures and Particle Acceleration in the Heliosphere”, by the US NSF AGS-1156094 (SHINE), and by NASA grant NNX14AI63G (Heliophysics Grandchallenge Theory), the MMS mission through grant NNX14AC39G, and the Solar Probe Plus science team (ISOIS/Princeton subcontract SUB0000165).

## REFERENCES

- AMBROSIANO, J., MATTHAEUS, W. H., GOLDSTEIN, M. L. & PLANTE, D. 1988 Test particle acceleration in turbulent reconnecting magnetic fields. *Journal of Geophysical Research* **93**, 14383–14400.
- BALE, S. D., KELLOGG, P. J., MOZER, F. S., HORBURY, T. S. & REME, H. 2005 Measurement of the Electric Fluctuation Spectrum of Magneto-hydrodynamic Turbulence. *Physical Review Letters* **94** (21), 215002.
- BIEBER, J. W. & MATTHAEUS, W. H. 1997 Perpendicular Diffusion and Drift at Intermediate Cosmic-Ray Energies. *The Astrophysical Journal* **485**, 655–659.
- BIRN, J., ARTEMYEV, A. V., BAKER, D. N., ECHIM, M., HOSHINO, M. & ZELENYI, L. M. 2012 Particle Acceleration in the Magnetotail and Aurora. *Space Science Reviews* **173**, 49–102.
- BRUNO, R. & CARBONE, V., ed. 2016 *Turbulence in the Solar Wind, Lecture Notes in Physics, Berlin Springer Verlag*, vol. 928.
- CADAVID, A. C., LAWRENCE, J. K., CHRISTIAN, D. J., JESS, D. B. & NIGRO, G. 2014 Heating mechanisms for intermittent loops in active region cores from aia/sdo euv observations. *The Astrophysical Journal* **795** (1), 48.
- CARGILL, P. J., VLAHOS, L., BAUMANN, G., DRAKE, J. F. & NORDLUND, Å. 2012 Current Fragmentation and Particle Acceleration in Solar Flares. *Space Science Reviews* **173**, 223–245.
- CARGILL, P. J., VLAHOS, L., TURKMANI, R., GALSGAARD, K. & ISLIKER, H. 2006 Particle Acceleration in a Three-Dimensional Model of Reconnecting Coronal Magnetic Fields. *Space Science Reviews* **124**, 249–259.
- CHANDRAN, B. D. G., LI, B., ROGERS, B. N., QUATAERT, E. & GERMASCHEWSKI, K. 2010 Perpendicular Ion Heating by Low-frequency Alfvén-wave Turbulence in the Solar Wind. *The Astrophysical Journal* **720**, 503–515.

- CHEN, SHIYI & KRAICHNAN, ROBERT H 1989 Sweeping decorrelation in isotropic turbulence. *Physics of Fluids A: Fluid Dynamics (1989-1993)* **1** (12), 2019–2024.
- DALENA, S., GRECO, A., RAPPAZZO, A. F., MACE, R. L. & MATTHAEUS, W. H. 2012 Magnetic moment nonconservation in magnetohydrodynamic turbulence models. *Phys. Rev. E* **86**, 016402.
- DECKER, R. B., KRIMIGIS, S. M., ROELOF, E. C. & HILL, M. E. 2010 Variations of Low-energy Ion Distributions Measured in the Heliosheath. In *American Institute of Physics Conference Series* (ed. J. Le Roux, G. P. Zank, A. J. Coates & V. Florinski), *American Institute of Physics Conference Series*, vol. 1302, pp. 51–57.
- DMITRUK, P., MATTHAEUS, W. H. & SEENU, N. 2004 Test Particle Energization by Current Sheets and Nonuniform Fields in Magnetohydrodynamic Turbulence. *The Astrophysical Journal* **617**, 667–679.
- DOBROWOLNY, M., MANGENEY, A. & VELTRI, P. 1980 Fully developed anisotropic hydromagnetic turbulence in interplanetary space. *Physical Review Letters* **45**, 144–147.
- DRAKE, J. F., OPPER, M., SWISDAK, M. & CHAMOUN, J. N. 2010 A Magnetic Reconnection Mechanism for the Generation of Anomalous Cosmic Rays. *The Astrophysical Journal* **709**, 963–974.
- DRAKE, J. F., SWISDAK, M., CHE, H. & SHAY, M. A. 2006 Electron acceleration from contracting magnetic islands during reconnection. *Nature* **443**, 553–556.
- FISK, L. A. & GLOECKLER, G. 2006 The Common Spectrum for Accelerated Ions in the Quiet-Time Solar Wind. *The Astrophysical Journal* **640**, L79–L82.
- FRANCI, L., LANDI, S., MATTEINI, L., VERDINI, A. & HELLINGER, P. 2015 High-resolution Hybrid Simulations of Kinetic Plasma Turbulence at Proton Scales. *The Astrophysical Journal* **812**, 21.
- FRISCH, URIEL 1995 *Turbulence*. Cambridge university press.
- GOSLING, J. T. 2010 Magnetic Reconnection in the Solar Wind: An Update. *Twelfth International Solar Wind Conference* **1216**, 188–193.
- GRAY, P. C. & MATTHAEUS, W. H. 1992 MHD turbulence, reconnection, and test-particle acceleration. In *Particle Acceleration in Cosmic Plasmas* (ed. G. P. Zank & T. K. Gaisser), *American Institute of Physics Conference Series*, vol. 264, pp. 261–266.
- GRECO, A., MATTHAEUS, W. H., SERVIDIO, S., CHUYCHAI, P. & DMITRUK, P. 2009a Statistical Analysis of Discontinuities in Solar Wind ACE Data and Comparison with Intermittent MHD Turbulence. *The Astrophysical Journal* **691**, L111–L114.
- GRECO, A., MATTHAEUS, W. H., SERVIDIO, S. & DMITRUK, P. 2009b Waiting-time distributions of magnetic discontinuities: Clustering or Poisson process? *Phys. Rev. E* **80** (4), 046401.
- GREEN, M. S. 1951 Brownian Motion in a Gas of Noninteracting Molecules. *The Journal of Chemical Physics* **19**, 1036–1046.
- HAUFF, T., PUESCHEL, M. J., DANNERT, T. & JENKO, F. 2009 Electrostatic and magnetic transport of energetic ions in turbulent plasmas. *Physical Review Letters* **102** (7), 075004.
- HAYNES, C. T., BURGESS, D. & CAMPOREALE, E. 2014 Reconnection and Electron Temperature Anisotropy in Sub-proton Scale Plasma Turbulence. *The Astrophysical Journal* **783**, 38.
- HOLMAN, G. D., SUI, L., SCHWARTZ, R. A. & EMSLIE, A. G. 2003 Electron Bremsstrahlung Hard X-Ray Spectra, Electron Distributions, and Energetics in the 2002 July 23 Solar Flare. *The Astrophysical Journal* **595**, L97–L101.
- HOSHINO, M., MUKAI, T., TERASAWA, T. & SHINOHARA, I. 2001 Superthermal electron acceleration in magnetic reconnection. *Journal of Geophysical Research* **106**, 25972.
- HOWES, GG, DORLAND, W, COWLEY, SC, HAMMETT, GW, QUATAERT, E, SCHEKOCHIHIN, AA & TATSUNO, T 2008 Kinetic simulations of magnetized turbulence in astrophysical plasmas. *Physical Review Letters* **100** (6), 065004.
- HUSSEIN, M & SHALCHI, A 2016 Simulations of energetic particles interacting with dynamical magnetic turbulence. *The Astrophysical Journal* **817** (2), 136.
- JOKIPII, J.R. 1966 Cosmic-ray propagation. i. charged particles in a random magnetic field. *The Astrophysical Journal* **146**, 480.
- JOKIPII, J.R. & PARKER, E.N. 1969 Stochastic aspects of magnetic lines of force with application to cosmic-ray propagation. *The Astrophysical Journal* **155**, 777.

- KOLMOGOROV, A. 1941 The Local Structure of Turbulence in Incompressible Viscous Fluid for Very Large Reynolds' Numbers. *Akademiia Nauk SSSR Doklady* **30**, 301–305.
- KUBO, R. 1957 Statistical-Mechanical Theory of Irreversible Processes. I. *Journal of the Physical Society of Japan* **12**, 570–586.
- LAZARIAN, A. & OPPER, M. 2009 A Model of Acceleration of Anomalous Cosmic Rays by Reconnection in the Heliosheath. *The Astrophysical Journal* **703**, 8–21.
- LE ROUX, J. A., ZANK, G. P., WEBB, G. M. & KHABAROVA, O. 2015 A Kinetic Transport Theory for Particle Acceleration and Transport in Regions of Multiple Contracting and Reconnecting Inertial-scale Flux Ropes. *The Astrophysical Journal* **801**, 112.
- LEPRETI, F., CARBONE, V., ABRAMENKO, V. I., YURCHYSHYN, V., GOODE, P. R., CAPPARELLI, V. & VECCHIO, A. 2012 Turbulent Pair Dispersion of Photospheric Bright Points. *The Astrophysical Journal* **759**, L17.
- LUO, H., KRONBERG, E. A., NYKYRI, K., TRATTNER, K. J., DALY, P. W., CHEN, G. X., DU, A. M. & GE, Y. S. 2017 IMF dependence of energetic oxygen and hydrogen ion distributions in the near-earth magnetosphere. *Journal of Geophysical Research: Space Physics* **122** (5), 5168–5180.
- MATTHAEUS, W. H. 1980 Wh matthaeus and d. montgomery, ann. ny acad. sci. 357, 203 (1980). *Ann. NY Acad. Sci.* **357**, 203.
- MATTHAEUS, W. H., QIN, G., BIEBER, J. W. & ZANK, G. P. 2003 Nonlinear collisionless perpendicular diffusion of charged particles. *The Astrophysical Journal Letters* **590** (1), L53.
- MATTHAEUS, W. H., AMBROSIANO, J. J. & GOLDSTEIN, M. L. 1984 Particle-acceleration by turbulent magnetohydrodynamic reconnection. *Physical Review Letters* **53**, 1449–1452.
- MATTHAEUS, W. H., GRAY, P. C., PONTIUS, JR., D. H. & BIEBER, J. W. 1995 Spatial Structure and Field-Line Diffusion in Transverse Magnetic Turbulence. *Physical Review Letters* **75**, 2136–2139.
- MATTHAEUS, W. H. & LAMKIN, S. L. 1986 Turbulent magnetic reconnection. *Physics of Fluids* **29**, 2513–2534.
- MATTHAEUS, W. H., SERVIDIO, S. & DMITRUK, P. 2008 Comment on “Kinetic Simulations of Magnetized Turbulence in Astrophysical Plasmas”. *Physical Review Letters* **101** (14), 149501.
- MILLER, J. A., GUESSOUM, N. & RAMATY, R. 1990 Stochastic Fermi acceleration in solar flares. *The Astrophysical Journal* **361**, 701–708.
- MILLER, J. A. & ROBERTS, D. A. 1995 Stochastic Proton Acceleration by Cascading Alfvén Waves in Impulsive Solar Flares. *The Astrophysical Journal* **452**, 912.
- NELKIN, M. & TABOR, M. 1990 Time correlations and random sweeping in isotropic turbulence. *Physics of Fluids A: Fluid Dynamics (1989-1993)* **2** (1), 81–83.
- OKA, M., PHAN, T.-D., KRUCKER, S., FUJIMOTO, M. & SHINOHARA, I. 2010 Electron Acceleration by Multi-Island Coalescence. *The Astrophysical Journal* **714**, 915–926.
- PARKER, E. N. 1957 Sweet's Mechanism for Merging Magnetic Fields in Conducting Fluids. *Journal of Geophysical Research* **62**, 509–520.
- PERRI, S., SERVIDIO, S., VAIVADS, A. & VALENTINI, F. 2017 Numerical Study on the Validity of the Taylor Hypothesis in Space Plasmas. *The Astrophysical Journal Supplement Series* **231**, 4.
- RAPPAZZO, A. F., MATTHAEUS, W. H., RUFFOLO, D., VELLI, M. & SERVIDIO, S. 2017 Coronal heating topology: The interplay of current sheets and magnetic field lines. *The Astrophysical Journal* **844** (1), 87.
- RICHARDSON, L. F. 1926 Atmospheric Diffusion Shown on a Distance-Neighbour Graph. *Proceedings of the Royal Society of London Series A* **110**, 709–737.
- RUFFOLO, D., MATTHAEUS, W. H. & CHUYCHAI, P. 2003 Trapping of Solar Energetic Particles by the Small-Scale Topology of Solar Wind Turbulence. *The Astrophysical Journal* **597**, L169–L172.
- RUFFOLO, D., MATTHAEUS, W. H. & CHUYCHAI, P. 2004 Separation of Magnetic Field Lines in Two-Component Turbulence. *The Astrophysical Journal* **614**, 420–434.
- RUFFOLO, D., PIANPANIT, T., MATTHAEUS, W. H. & CHUYCHAI, P. 2012 Random Ballistic Interpretation of Nonlinear Guiding Center Theory. *The Astrophysical Journal Letters* **747**, L34.

- SERVIDIO, S., CARBONE, V., DMITRUK, P. & MATTHAEUS, W. H. 2011a Time decorrelation in isotropic magnetohydrodynamic turbulence. *EPL (Europhysics Letters)* **96**, 55003.
- SERVIDIO, S., GRECO, A., MATTHAEUS, W. H., OSMAN, K. T. & DMITRUK, P. 2011b Statistical association of discontinuities and reconnection in magnetohydrodynamic turbulence. *Journal of Geophysical Research (Space Physics)* **116**, A09102.
- SERVIDIO, S., HAYNES, C. T., MATTHAEUS, W. H., BURGESS, D., CARBONE, V. & VELTRI, P. 2016 Explosive particle dispersion in plasma turbulence. *Phys. Rev. Lett.* **117**, 095101.
- SERVIDIO, S., MATTHAEUS, W. H., SHAY, M. A., CASSAK, P. A. & DMITRUK, P. 2009 Magnetic Reconnection in Two-Dimensional Magnetohydrodynamic Turbulence. *Physical Review Letters* **102** (11), 115003.
- SERVIDIO, S., VALENTINI, F., PERRONE, D., GRECO, A., CALIFANO, F., MATTHAEUS, W. H. & VELTRI, P. 2015 A kinetic model of plasma turbulence. *Journal of Plasma Physics* **81** (1), 325810107.
- SHALCHI, ANDREAS 2015 Perpendicular diffusion of energetic particles in collisionless plasmas. *Physics of Plasmas (1994-present)* **22** (1), 010704.
- SHALCHI, A. & DOSCH, A. 2008 Nonlinear Guiding Center Theory of Perpendicular Diffusion: Derivation from the Newton-Lorentz Equation. *The Astrophysical Journal* **685**, 971–975.
- SHEBALIN, J. V., MATTHAEUS, W. H. & MONTGOMERY, D. 1983 Anisotropy in MHD turbulence due to a mean magnetic field. *Journal of Plasma Physics* **29**, 525–547.
- STONE, E. C., CUMMINGS, A. C., McDONALD, F. B., HEIKKILA, B. C., LAL, N. & WEBBER, W. R. 2008 An asymmetric solar wind termination shock. *Nature* **454**, 71–74.
- SUBEDI, P., SONSETTEE, W., BLASI, P., RUFFOLO, D., MATTHAEUS, W.H., MONTGOMERY, D., CHUYCHAI, P., DMITRUK, P., WAN, M., PARASHAR, T.N. & CHHIBER, R. 2017 Charged particle diffusion in isotropic random magnetic fields. *The Astrophysical Journal* **837**, 140.
- TAYLOR, G. I. 1922 *Proc. London Math. Soc.* **20**, 196.
- TAYLOR, J. B. & MCNAMARA, B. 1971 Plasma Diffusion in Two Dimensions. *Physics of Fluids* **14**, 1492–1499.
- TESSEIN, J. A., MATTHAEUS, W. H., WAN, M., OSMAN, K. T., RUFFOLO, D. & GIACALONE, J. 2013 Association of Suprathermal Particles with Coherent Structures and Shocks. *The Astrophysical Journal* **776**, L8.
- ZANK, G. P., LE ROUX, J. A., WEBB, G. M., DOSCH, A. & KHABAROVA, O. 2014a Particle Acceleration via Reconnection Processes in the Supersonic Solar Wind. *The Astrophysical Journal* **797**, 28.
- ZANK, G. P., LE ROUX, J. A., WEBB, G. M., DOSCH, A. & KHABAROVA, O. 2014b Particle Acceleration via Reconnection Processes in the Supersonic Solar Wind. *The Astrophysical Journal* **797**, 28.